Effects of gap and band anisotropy on spin susceptibility in the oxide superconductors

J. M. Rendell and J. P. Carbotte
Department of Physics and Astronomy, McMaster University, Hamilton, Ontario, Canada L8S 4M1
(Received 21 September 1995)

We have studied the momentum space anisotropy present in the imaginary part of the spin susceptibility when an extended *s*-wave component ($s_{x^2+y^2}$) is added to the *d*-wave ($d_{x^2-y^2}$) superconducting gap. It is found that as the amount of the extended *s*-wave component is increased, the two pairs of incommensurate nesting peaks begin to differ increasingly in height and shape. In addition, band structure anisotropy, which in contrast to gap anisotropy would be present even in the normal state, is also discussed.

I. INTRODUCTION

Important spin fluctuation effects are present in the superconducting state of the copper oxides and some theories[1–4] invoke the presence of this magnetism as the mechanism responsible for superconductivity although, at the moment, there is no consensus on this point.[5–7] The superconducting and normal state spin susceptibility has been extensively studied in LaSrCuO and YBaCuO by inelastic neutron scattering[8–23] and many theoretical papers[24–44] exist on the subject.

There are now many experiments indicating that the gap in some of the high-T_c oxides has $d_{x^2-y^2}$ symmetry.[45,46] As an example, the linear temperature dependence (T) of the low temperature penetration depth observed in high quality $YBa_2Cu_3O_{7}$ single crystals[47–51] as well as its switch over to a T^2 dependence[52] on Zn doping of the CuO_2 planes, is easily and naturally interpreted as due to a *d*-wave gap. Also, high resolution ($\sim$10 meV) angular resolved photo emission experiments (ARPES) in $Bi_2Sr_2CaCu_xO_{8+\delta}$ have indicated a near zero gap on the Fermi surface in the two diagonal directions with a maximum in the direction towards the faces[53–61] of the square CuO_2 Brillouin zone. This observation is also consistent with $d_{x^2-y^2}$ symmetry. On the other hand, other ARPES data have given instead zeros[62] on either side of the diagonals displaced by approximately 10°. These results have found a straightforward interpretation in terms of a gap with s_{xy} symmetry. Nevertheless, on the whole, the evidence for *d*-wave symmetry is strong.

Penetration depth and ARPES experiments are not sensitive to the phase of the gap and depend only on its absolute value so that a unique and definitive assignment of $d_{x^2-y^2}$ symmetry is not possible from such data alone. To clarify this point, several experiments have been designed to observe directly the phase of the gap[63–65] although, again, not all agree on assignment of $d_{x^2-y^2}$ symmetry. Thus the situation remains controversial and other points of view exist[66–68] but here we will assume a *d*-wave gap.

Another important feature of the copper oxides that needs to be considered, however, is that some are not tetragonal. For example, $YBa_2Cu_3O_7$ has chains along a definite direction so that this compound is clearly orthorhombic. A direct consequence of this is that the in-plane resistivity[69] and thermal conductivity[70] are quite anisotropic. Recently, a very large anisotropy has also been observed in the penetration depth which is 1600 Å in the *a* direction as compared with 1030 Å in the *b* direction[71] in untwinned single crystal samples.

A possible model for the superconductivity in the oxides with a gap that has $d_{x^2-y^2}$ symmetry is the nearly antiferromagnetic Fermi liquid model (NAFFLM). In this model, pairing proceeds through coupling to the spin fluctuation which can be described by a phenomenological susceptibility as done by Millis, Monien, and Pines (MMP) (Ref. 1) which they determined from a consideration of NMR data. This model, which applies to tetragonal systems with pure *d*-wave gap, was extended to include an orthorhombic band structure by O'Donovan *et al.*[72,73] and Branch *et al.*[74] In this case, the BCS gap equation with MMP susceptibility leads quite directly to a mixed symmetry solution for the superconducting gap which includes an extended $s_{x^2+y^2}$ component as well as the more usual $d_{x^2-y^2}$ part. The fast Fourier transform numerical solutions of the BCS equation obtained in this extended model contain many higher harmonics of these two irreducible representations of the tetragonal crystal lattice point group. However, for most purposes, the physics of the situation is captured by including only the lowest harmonic of each of the two irreducible representations, $s_{x^2+y^2}$ and $d_{x^2-y^2}$.

In this paper, we calculate the electron spin susceptibility of a single band two-dimensional CuO_2 tight binding plane in a random phase approximation including Stoner enhancement which is due to correlation effects described by the Hubbard U. We study, in particular, the effect of adding on an extended *s*-wave component to the gap besides its more usual $d_{x^2-y^2}$ part. We also study the direct effect on the spin susceptibility of an orthorhombic distortion in the band structure. For this purpose, we stay, for simplicity, within a single band model but include a different first nearest-neighbor hopping in *a* and *b* directions. This distortion can be thought of as a simplified way to emulate the existence of the chains in YBCO so that the one band Fermi surface no longer has tetragonal symmetry. Of course, this is a very simplified model. In actuality, the Fermi surface of YBCO has several sheets; two CuO_2-like and one chainlike with hybridization between them.[75–81] Still, our simplified model is capable of including orthorhombicity whatever its source and will be sufficient for our purpose here. The model has been successfully applied[72,73] to a discussion of the observed penetration depth anisotropy[71,73] in YBCO and the size of the

Josephson critical current [65,74] seen between YBCO and Pb for tunneling along the c axis.

In Sec. II, we give the necessary formalism. Numerical results are to be found in Sec. III and a conclusion in Sec. IV.

II. FORMALISM

The bare single spin susceptibility in the superconducting state for momentum transfer $\mathbf{q}$ and energy ω is given by

$$\chi_0(\mathbf{q};\omega)=\frac{1}{2\Omega}\sum_k \left\{ a_+(\mathbf{k},\mathbf{q})\frac{f(E_{\mathbf{k}+\mathbf{q}})-f(E_{\mathbf{k}})}{\omega-(E_{\mathbf{k}+\mathbf{q}}-E_{\mathbf{k}})+i\Gamma} + \frac{1}{2}a_-(\mathbf{k},\mathbf{q})\frac{1-f(E_{\mathbf{k}+\mathbf{q}})-f(E_{\mathbf{k}})}{\omega+(E_{\mathbf{k}+\mathbf{q}}+E_{\mathbf{k}})+i\Gamma} + \frac{1}{2}a_-(\mathbf{k},\mathbf{q})\frac{f(E_{\mathbf{k}+\mathbf{q}})-f(E_{\mathbf{k}})-1}{\omega-(E_{\mathbf{k}+\mathbf{q}}+E_{\mathbf{k}})+i\Gamma}\right\},$$

$$a_\pm(\mathbf{k},\mathbf{q})=1\pm\frac{\epsilon_{\mathbf{k}+\mathbf{q}}\epsilon_{\mathbf{k}}+\Delta_{\mathbf{k}+\mathbf{q}}\Delta_{\mathbf{k}}}{E_{\mathbf{k}+\mathbf{q}}E_{\mathbf{k}}}, \tag{1}$$

where $f(x)$ is the Fermi Dirac distribution function at finite temperature (T) and Γ is a damping factor needed to control the singularities in the denominators and taken to be $\Gamma=0.01t$ or $0.05t$ in the numerical data present in this paper. The full spin susceptibility in random phase approximation, enhanced by the Coulomb interactions, which we denote by $\chi(\mathbf{q};\omega)$, is given by

$$\chi(\mathbf{q};\omega)=\frac{\chi_0(\mathbf{q};\omega)}{1-U\chi_0(\mathbf{q};\omega)}, \tag{2}$$

where U is the Hubbard U which accounts for correlations. The antiferromagnetic transition occurs when the denominator of Eq. (2) vanishes and so the susceptibility goes to infinity. This occurs at a particular value of momentum $\mathbf{q}$ denoted by $\mathbf{q}_c$ (critical) and defines a critical value of U denoted by U_c which is given by $U_c=1/\chi_0(\mathbf{q}_c\omega)$ for momentum $\mathbf{q}_c$ and energy transfer ω. In Eq. (1), Ω is a normalizing volume, the sum is over momentum in the first Brillouin zone of the CuO_2 plane which is taken to be tetragonal. The superconducting energy gap is $\Delta_{\mathbf{k}}$ and the quasiparticle energies $E_{\mathbf{k}}\equiv\sqrt{\epsilon_k^2+\Delta_k^2}$ where $\epsilon_{\mathbf{k}}$ is the normal state electronic dispersion.

In this paper, we will be interested in a gap which is a combination of the two lowest harmonics of the $d_{x^2-y^2}$ and $s_{x^2+y^2}$ irreducible representations of the two-dimensional CuO_2 tetragonal plane. They are

$$d_{x^2-y^2}\equiv\cos(k_x)-\cos(k_y) \tag{3}$$

and

$$s_{x^2+y^2}\equiv\cos(k_x)+\cos(k_y), \tag{4}$$

where k_x and k_y are momentum components in x and y direction, respectively. The gap then has the form

$$\Delta_{\mathbf{k}}=\Delta_d[\cos(k_x)-\cos(k_y)]+\Delta_s[\cos(k_x)+\cos(k_y)]. \tag{5}$$

In our previous numerical solutions[72–74] of the BCS gap equations using fast Fourier transforms, a numerical technique which places no restrictions on the symmetry of the resulting gap, we have found that, for an orthorhombic system in a single band model, many higher harmonics are present besides those of Eqs. (3) and (4). But for most purposes, this is not important and qualitative correct results can be obtained on the basis of Eq. (5) alone. The BCS gap equation that is solved to get such mixed representation solutions[72–74] is based on the phenomenological spin susceptibility $\chi_{\mathbf{k}-\mathbf{k}'}$ determined in the work of Millis, Monien, and Pines[1] (MMP) and tight-binding electronic dispersions of the form

$$\epsilon_{\mathbf{k}}=-2t[\cos(k_x)+(1+\delta)\cos(k_y)-2B\cos(k_x)\cos(k_y)]-\mu, \tag{6}$$

where t is the first nearest-neighbor hopping, δ is an anisotropy parameter which breaks tetragonal symmetry and makes the x and y directions distinct, B is a second nearest-neighbor hopping parameter, and μ is the chemical potential in units of t. It is related to the filling factor $\langle n\rangle$ given by

$$\langle n\rangle=\frac{1}{2\Omega}\sum_{\mathbf{k}}\left[1-\frac{\epsilon_{\mathbf{k}}}{E_{\mathbf{k}}}\tanh\left(\frac{E_{\mathbf{k}}}{2k_BT}\right)\right], \tag{7}$$

where half-filling (single spin) corresponds to $\langle n\rangle=0.5$. In Eq. (7), T is temperature, as before, and k_B is the Boltzmann factor.

The single orthorhombic two-dimensional band structure model of Eq. (6) is, of course a simplification but it does allow us to treat, in a simple fashion, an orthorhombic situation with gap of the form (5) which has an $s_{x^2+y^2}$ as well as $d_{x^2-y^2}$ component. For YBCO, Eq. (6) is intended to represent the combined system of planes and chains. Of course, in a complete model, the Fermi surface has several sheets rather than a single one, with one sheet related mainly to the chains and two to the planes. This complication is beyond the scope of our study here.

The numerical evaluation of Eq. (1) for a particular admixture of $s_{x^2+y^2}$ and $d_{x^2-y^2}$ [Eq. (5)] proceeds through a numerical sampling of the irreducible part of the Brillouin zone involving N^2 sampling points. For all runs to be presented here, the filling was fixed at $\langle n\rangle=0.4$ for illustrative purposes only. As the parameters in the electronic dispersion relation (6) are varied, the chemical potential required to keep $\langle n\rangle$ at 0.4, of course, changes. We will consider cases with second nearest-neighbor $B=0$ and others with $B=0.45$ which are roughly appropriate to the band structure of LaSrCuO and YBaCuO, respectively. Several values of the band structure anisotropy parameter δ of Eq. (6) were considered but only $\delta=0.25$ is given here. In all runs reported, we have used $\Gamma=0.01t$ or $0.05t$ and a neutron energy transfer $\omega=0.05t$ unless otherwise stated. The maximum gap value at $T=0$ was set at $2\Delta_0=0.4t$ and the critical temperature at $T_c=0.1t$, corresponding to $T\sim100$ K. This is the temperature at which normal state results are presented.

III. NUMERICAL RESULTS

We start with the tetragonal case for the band structure dispersion relation of Eq. (6), i.e., $\delta=0$. The four frames of Fig. 1 give the imaginary part of the single spin susceptibility of Eq. (2) $[\chi(\mathbf{q},\omega)]$ as a function of momentum transfer $\mathbf{q}$ for a fixed energy transfer $\omega=0.05t$. In this figure, q_x/π ranges

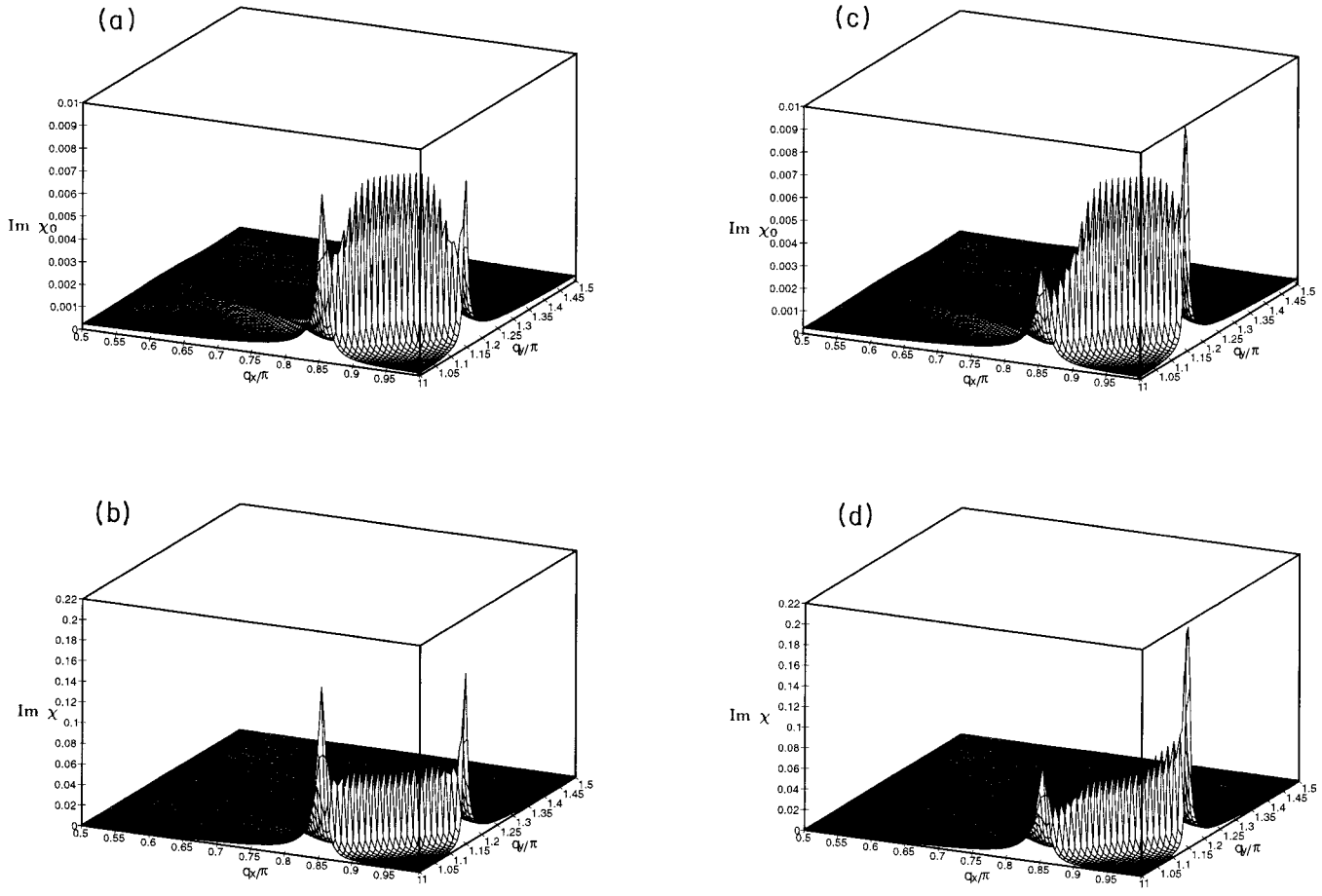

FIG. 1. The common parameters are critical temperature $T_c=0.1t$, maximum gap $2\Delta_0=4T_c$, filling $\langle n\rangle=0.4$, second nearest-neighbor hopping $B=0$ on a tetragonal lattice, neutron energy $\omega=0.05t$, and smearing parameter $\Gamma=0.01t$. The number of points used in the Brillouin zone is $(330)^2$. Frames (a) and (b) involve pure d-wave gap and give the imaginary part of the spin susceptibility as a function of momentum q_x and q_y in the two-dimensional reciprocal space of the copper oxide planar lattice. In frame (a), the Coulomb parameter $U=0$, while in frame (b) it is equal to $2.0t$ with critical value $\sim 2.52t$. Frames (c) and (d) involve 20% $s_{x^2+y^2}$ (extended s wave) and 80% $d_{x^2-y^2}$ (d wave) otherwise they are the same as (a) and (b) with $U_c\cong 2.50t$.

from 0.5 to 1 and q_y/π from 1 to 1.5; so (π,π) is the right, front corner. The temperature is taken to be zero and the state is superconducting. Frame 1(a) is for a gap with pure $d_{x^2-y^2}$ symmetry [Eq. (3)] and applies to the case when the Coulomb repulsion in Eq. (2) is set to zero so that it is the bare susceptibility of Eq. (1), $\chi_0(\mathbf{q};\omega)$ that is displayed. Note that the results are consistent with tetragonal symmetry. There are four identical symmetrically placed nesting peaks on the Brillouin zone face connected by prominent narrow ridges which come from gap node to gap node scattering. The geometrical origin of these gap node features, which reflect the Fermi surface shape and the symmetry of the gap, will shortly be emphasized further when we refer to Fig. 2. Frame 1(b) uses a finite value of Coulomb repulsion $U=2.0t$ in Eq. (2) otherwise the parameters are the same as for frame 1(a) (pure $d_{x^2-y^2}$ symmetry). The critical value of U is estimated to be $U_c=2.52t$. This value, which is quoted only for information, corresponds to the antiferromagnetic phase transition boundary. On comparing frame 1(b) with frame 1(a), we note first the large change in scale on the vertical axis. It ranges up to 0.010 for the noninteracting case [frame 1(a)] with $U=0$ and up to 0.22 for the exchanged, enhanced finite U case [frame 1(b)]. This large enhancement of the spin susceptibility comes from the denominator in Eq. (2) which can become small as the antiferromagnetic boundary is approached. Note that when a finite U is included, the susceptibility χ of Eq. (2) involves both real and imaginary parts of the noninteracting $\chi_0(\mathbf{q};\omega)$ of Eq. (1). As U is increased further towards the antiferromagnetic phase boundary, χ will, of course, become even more enhanced and eventually diverge. Values of U near U_c correspond to the NAFFLM which envisages large Stoner enhancements of the bare spin susceptibility $\chi_0(\mathbf{q};\omega)$ of Eq. (1) and very significant magnetic effects in the superconducting state. On comparing frame 1(b) with frame 1(a), it should also be noted that the four nesting peaks, which remain symmetric in placement, shape, and height, have become much more prominent and the gap node scattering ridges are now not quite as large in relation to the

peak values. The figure remains tetragonal, of course, because we have used a tetragonal lattice and a pure $d_{x^2-y^2}$ gap function [Eq. (3)]; a finite value of U does not change this symmetry.

In the next two frames (c) and (d) of Fig. 1, a tetragonal lattice is retained but the gap admixture in Eq. (5) is taken to be 20% $s_{x^2+y^2}$ and 80% $d_{x^2-y^2}$. The parameters Δ_s and Δ_d include these factors, respectively, as well as the temperature dependent gap function $\Delta_0(T)$. An important result is that the nesting peaks, which are still quite prominent in both frames 1(c) and 1(d), have become asymmetric. They now come in pairs with each pair having a different height (though the position remains symmetric). The gap ridges between these incommensurate nesting peaks also show asymmetry. As in the case of the previous two frames, inclusion of a finite Coulomb repulsion in frame 1(d) as compared with frame 1(c), which is for $U=0$, reduces the relative size of the gap ridges as compared to the size of the incommensurate nesting points and increases very slightly the anisotropy of the height of the nesting peaks in the figure. In frame 1(d), $U=2t$ and the critical value of U is $U_c=2.50t$ The admixture of a 20% $s_{x^2+y^2}$ component to the gap in Eq. (5) has slightly shifted the value of the critical value of U, i.e., U_c which corresponds to the antiferromagnetic phase boundary. It is clear from this figure that it should be possible, in principle at least, to fix the amount of $s_{x^2+y^2}$ admixture from the difference in peak height seen in the superconducting state of the two pairs of incommensurate nesting peaks. This anisotropy will show up only in the superconducting state and will not be present in the normal state. When the gap is zero, the system has tetragonal symmetry and nesting peaks are symmetric as in frames (a) and (b) of Fig. 1. This anisotropy appears to be present in the superconducting state data of Mason *et al.*[20] in LaSrCuO.

Figure 2 consists of five frames labeled from (a) to (e) and involves a tetragonal lattice [$\delta=0$ in Eq. (6)] with next-nearest-neighbor $B=0$. This is a reasonable model for the band structure of LaSrCuO. As in Fig. 1, the filling is set at $\langle n\rangle=0.4$ and the width $\Gamma=0.01t$, the frequency $\omega=0.05t$, and the number of sampling points in the Brillouin zone is N^2 with $N=1002$. Frame 2(a) shows the closed Fermi surface contour (solid line). It is squarelike with flat regions perpendicular to the main diagonals of the first Brillouin zone. The dotted lines show the nesting ridges which reflect the geometry of the Fermi surface. They are conveniently shown in an extended Brillouin zone, centered around $\mathbf{q}=(\pi,\pi)$. Lavagna *et al.*[33,35] refers to these nesting ridges as dynamic Kohn anomalies. Their geometrical construction is as follows: take all vectors connecting the Fermi surface to itself going through the origin (Γ point) and displace the resulting vector parallel to itself up to the origin of the first Brillouin zone. The set of all momenta transfers that map the Fermi surface on to itself through the Γ point (0,0) are shown as dotted lines (nesting ridges) in the extended Brillouin zone. The nesting peaks correspond to the intersection of two nesting ridges which enhance these particular Fermi surface to Fermi surface transitions and lead to peaks in the spin susceptibility. These nesting ridges and peaks can be seen in the imaginary part of the spin susceptibility at $T=0$, when there is no Coulomb potential U. Then the peaks have exactly twice the height of the ridges. As the potential is turned on, the nesting peaks are enhanced more than the ridges. Also shown on the same figures is the position of the center of the gap node to gap node scattering structures. These exist only in the superconducting case, must be positioned on the nesting ridges, and consist of the same nesting transition just described but involve only those that also go from gap node to gap node. For the pure $d_{x^2-y^2}$ case, the point (open circle) falls directly between the two nesting peaks and on the nesting ridge. This peak moves off along the nesting ridge (to the right) as an admixture of $s_{x^2+y^2}$ is introduced and to the right of the open circle. The asterisk is for a 20% admixture of $s_{x^2+y^2}$ component in Eq. (5), the second open circle, which falls right on the nesting peak (π,q_y), is for 50% $s_{x^2+y^2}$, and finally, the last point (a second asterisk) is for 80% $s_{x^2+y^2}$ and 20% $d_{x^2-y^2}$. We stress again that these gap peaks exist only in the superconducting state and result from scattering between gap nodes on the Fermi surface. In frame 2(a), the gap node to gap node peaks are only shown in one direction. In reality, there are three more sets symmetrically positioned. The relative height of the gap node peak is strongly affected by temperature, T, the smearing, Γ, and the Coulomb potential, U.

In frame (b) of Fig. 2, we show a plot of the imaginary part of the spin susceptibility $\chi_0(\mathbf{q},\omega)$ for $\omega=0.05t$ and $\mathbf{q}$ along a line going through two of the nesting peaks. The horizonal axis is q_x/π along $q_y=\pi$ with first nesting peak at 0.85; the second then falls at 1.0 by arrangement. The position of these peaks is, of course, completely dependent on the Fermi surface geometry and will change with filling and any change in the dispersion relation (6). The lower curve of frame 2(b) applies to the superconducting state at zero temperature and the upper curve to the normal state at T_c, taken to be 100 K. The two incommensurate nesting peaks are sharper but much narrower in the superconducting case, and the gap node peak, which falls exactly halfway between the two nesting peaks, is clearly seen in the lower curve. This frame applies to the pure *d*-wave case and exhibits tetragonal symmetry. This is in contrast to the results shown in frame 2(c), which are based on a 20% admixture of $s_{x^2+y^2}$ in the gap function with 80% $d_{x^2-y^2}$. The position of the nesting peaks has not changed but now they no longer have the same height and shape. Also, the gap node peak is asymmetric and its maximum has moved away from the smaller peak and closer to the higher nesting peak as shown in frame (a). Increasing U will give bigger peaks, but not increase by much the difference in height. The next frame 2(d) shows the nesting peaks with a 50% $d_{x^2-y^2}$ and 50% $s_{x^2+y^2}$ gap. Now the gap scattering peak is at the same position as the right hand nesting peak, but the two contributions are clearly distinguished. Increasing U will produce larger peaks ad make the right hand peak bigger with respect to the left hand peak. This is due to the presence of the gap node scattering peak. The last frame 2(e) shows the case of 20% $d_{x^2-y^2}$ and 80% $s_{x^2+y^2}$. The gap scattering peak is now seen to the right of the right hand nesting peak. The gap scattering peak is broad along the nesting ridge and falls away rapidly in the perpendicular direction. If the chosen line in momentum space does not pass directly through the position of the gap scattering peak, the shape seen will not be fully representative. This is the case in frame 2(d). The nesting ridges curve away from the line joining the two nesting peaks. Adding a Coulomb en-

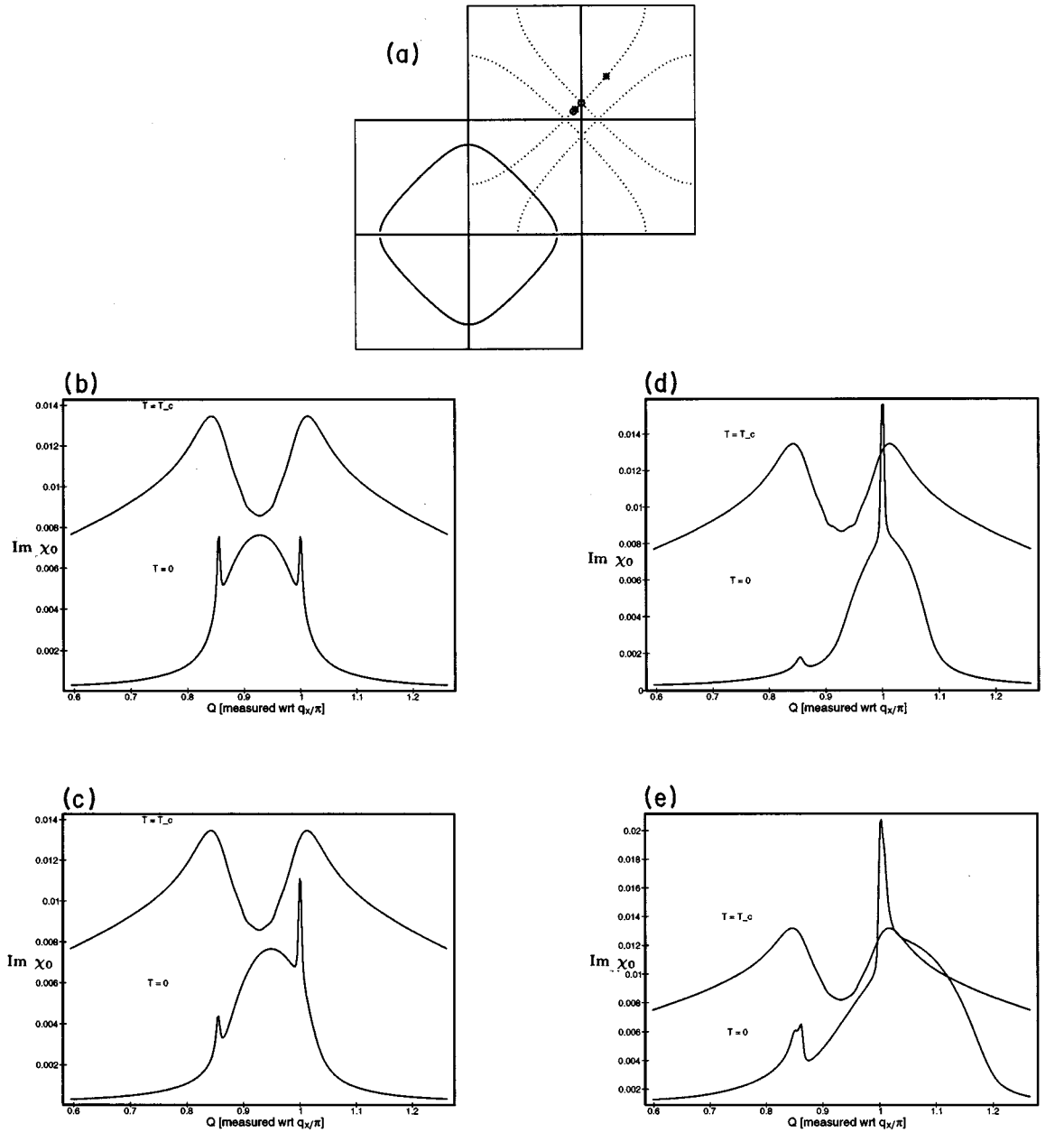

FIG. 2. The common parameters are critical temperature $T_c=0.1t$, maximum gap $2\Delta_0=4T_c$, filling $\langle n\rangle=0.4$, second nearest-neighbor hopping $B=0$, neutron energy transfer $\omega=0.05t$, and smearing parameter $\Gamma=0.01t$; $\pi=501$ points. Frame (a) gives the Fermi surface at a filling of $\langle n\rangle=0.4$ (solid, closed curve) and the nesting ridges (dotted curves). The intersection of two nesting ridges give the position of the nesting peaks. Also shown are the gap node peak positions as ○'s for pure *d*-wave and 50% extended *s*-wave admixture and ×'s for 20% and 80% extended *s*-wave admixture. All other frames give the imaginary part of the spin susceptibility as a function of momentum along the line $(0.59\pi, 0.74\pi)$ to $(1.26\pi, 1.41\pi)$ for frames (b), (c), (d), and (e), which correspond to pure *d* wave, a 20% extended *s* wave, 50% $s_{x^2-y^2}$, and 80% $s_{x^2+y^2}$, respectively, with zero value for the Coulomb potential *U*. Two temperatures, $T=T_c$ (usually upper line) and $T=0$, are plotted in each frame. Note in frame (d) that the gap peak and the nesting peak coincide, but the shapes are clearly distinguishable.

hancement to these examples reduces the relative height of the gap scattering peak.

In Fig. 3, we show our results for the imaginary part of the susceptibility $\mathrm{Im}\chi(Q;\omega)$ for $U=2.0t, \langle n\rangle=0.4$, $\omega=0.05t$, $\Gamma=0.05t$, $\delta=0$, $B=0$, $N^2=(330)^2$, along the q_y axis with $q_x=\pi$ (upper curve in each pair) and along q_x with $q_y=\pi$ (lower curve), so as to emphasize the anisotropy not only in the height of the incommensurate nesting peak but also in its shape. For the convenience of the reader, each set of two profiles is displaced upward in the figure by a constant amount along the vertical axis. The lowest curve is for the normal state at temperature $T=0.1t$ and is included for comparison. It is symmetric, i.e., identical in *x* and *y* direction because the system is tetragonal [$\delta=0$ in Eq. (6)]. The second lowest set of two curves also shows tetragonal symmetry. They apply to the superconducting state at zero tem-

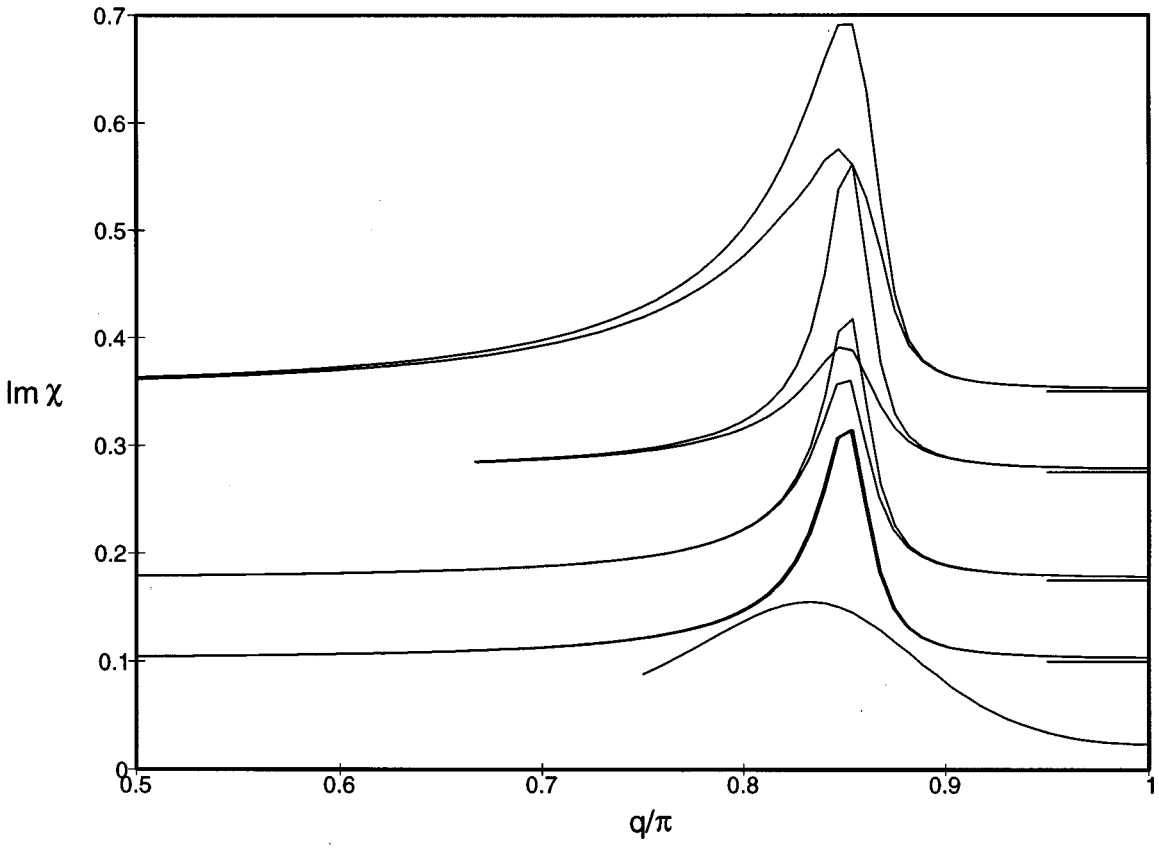

FIG. 3. The parameters are critical temperature $T_c=0.1t$, maximum gap $2\Delta_0=4T_c$, filling $\langle n\rangle=0.4$, second nearest-neighbor hopping $B=0$, neutron energy transfer $\omega=0.05t$, and smearing parameters $\Gamma=0.05t$ (tetragonal case). The number of points used in the Brillouin zone was $(288)^2$ in all cases except the normal state which has $(256)^2$ points. The lowest curve is the normal state at $T=T_c$. The others are at $T=0$. From bottom to top, each pair of curves is displaced by 0.1 units on the vertical axis. The imaginary part of the spin susceptibility is plotted as a function of momentum q_x with $q_y=\pi$ (upper line in pair) and q_y with $q_x=\pi$ (lower line in pair). From bottom to top, normal state, d wave, 20% $s_{x^2+y^2}+80\%$ $d_{x^2-y^2}$, 50% $s_{x^2+y^2}+50\%$ $d_{x^2-y^2}$, 80% $s_{x^2+y^2}+20\%$ $d_{x^2-y^2}$.

perature $T=0$ and a pure $d_{x^2-y^2}$ gap which preserves the tetragonal symmetry. Once some admixture of $s_{x^2+y^2}$ (20%, 50%, and 80%, respectively, for the last three sets of curves) is included, this symmetry is lost and the profiles become distorted. The curves for the spin susceptibility then differ between x and y direction. This anisotropy has its origin solely in the gap admixture, i.e., the mixing of $s_{x^2+y^2}$ and $d_{x^2-y^2}$ symmetries and not in the band structure anisotropy. In the corresponding normal state, the profiles are symmetric and the anisotropy referred to appears only in the superconducting state. This is the clear signature of the admixing of $s_{x^2+y^2}$ symmetry into an otherwise $d_{x^2-y^2}$ gap function.

In Fig. 4, we examine the effect of including a next-nearest-neighbor hopping in the electronic dispersion (6) but still retain tetragonal symmetry, i.e., the band structure anisotropy parameter $\delta=0$ in Eq. (6). Four frames are presented. In frame 4(c), we show the Fermi surface (solid curve) at filling $\langle n\rangle=0.4$. As shown, the Fermi contours are open, but they can be reassembled about $q=(\pi,\pi)$ to form a closed figure which then looks much like that of frame (a) in Fig. 2 but rotated by 45% compared with the $B=0$ case (LaSrCuO). Here $B=0.45$ which is more representative of the Fermi surface of YBaCuO. The dashed dotted lines shown in the first Brillouin zone are the lines of zero gap for the case 20% $s_{x^2+y^2}$ and 80% $d_{x^2-y^2}$. This is to be contrasted to the pure $d_{x^2-y^2}$ case for which the gap nodes are on the main diagonals of the Brillouin zone. The dotted curves shown in an extended Brillouin zone with center at (π,π) are the nesting ridges which cross to give the four nesting peaks positioned on the Brillouin zone boundaries. The center of the gap node to gap node scattering peaks are indicated by an $(\times)$ for the pure $d_{x^2-y^2}$ case and by an open circle $(\bigcirc)$ for the 20% $s_{x^2+y^2}$ case. Note that this peak is symmetrically placed between the nesting peaks in the pure d-wave case while it moves to an asymmetric position as a contribution of $s_{x^2+y^2}$ is mixed into the gap function. Frames 4(a), 4(b), and 4(d), give the imaginary part of the spin susceptibility as a function of momentum (q_x,q_y) and are for energy $\omega=0.05t$, maximum gap of $2\Delta_0=0.4t$, $\Gamma=0.05t$, $T_c=0.1t$, and $U=2.5t$. The mesh has $(288)^2$ points in the first Brillouin zone. Frame 4(a) gives normal state results at $T=0$ with $U_c=2.52t$. The incommensurate nesting peaks are clearly seen and remain symmetric because the inclusion of a finite value for B in Eq. (6) does not lift the tetragonal symmetry of the system. The third peak (background) in frame 4(a) appears only in the normal state with nonzero B. Frame 4(b) shows similar re-

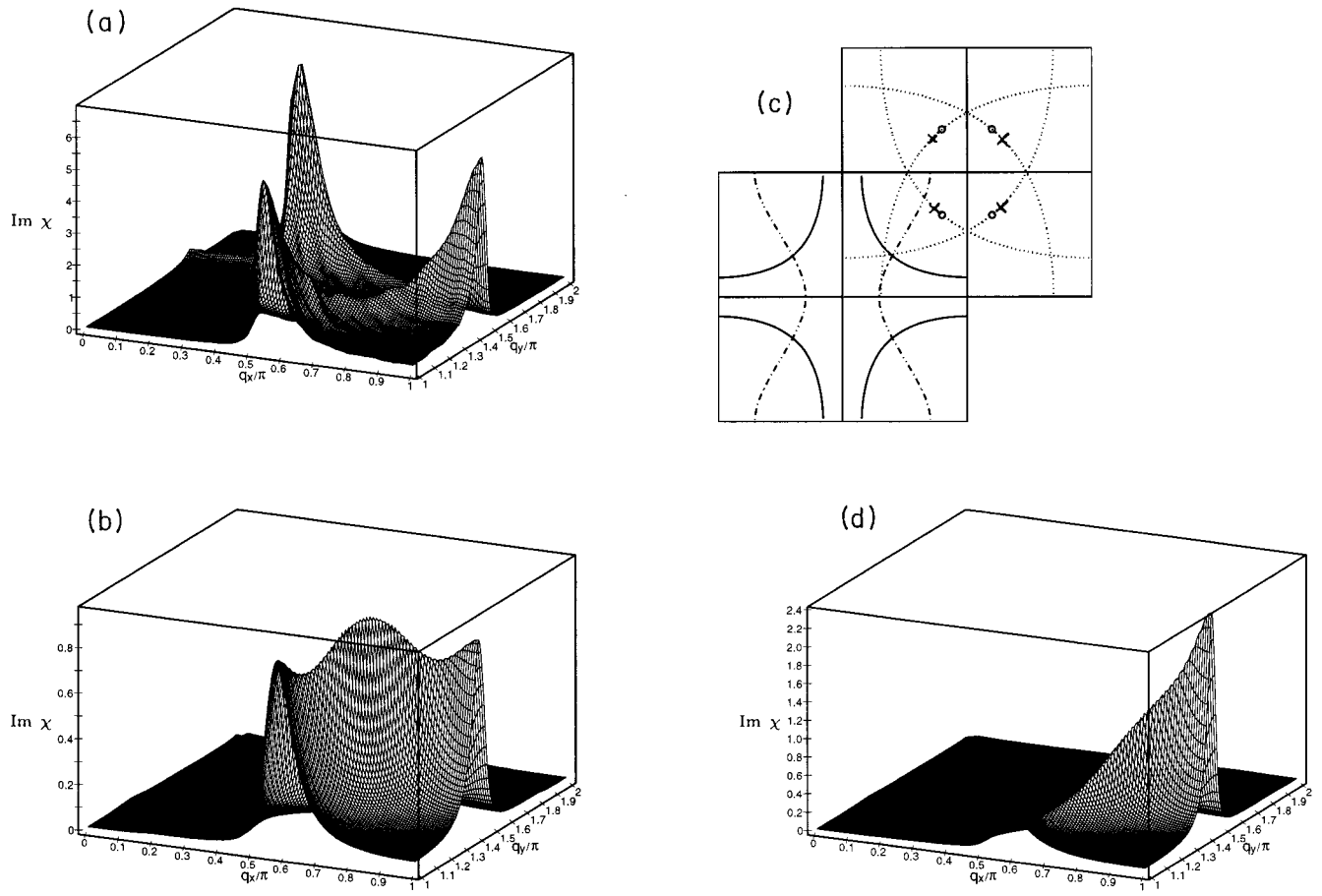

FIG. 4. The parameters are critical temperature $T_c=0.1t$, maximum gap $2\Delta_0=4T_c$, filling $\langle n\rangle=0.4$, second nearest-neighbor hopping $B=0.45$, neutron energy transfer $\omega=0.05t$, and smearing parameter $\Gamma=0.05t$. The number of points used in the Brillouin zone is $(288)^2$. Frames (a), (b), and (d) give the imaginary part of the spin susceptibility as a function of momentum (q_x,q_y) in the Brillouin zone at $T=0$, with Coulomb parameter $U=2.5t$. Frame (c) gives the Fermi surface (solid curves), the gap node line for 20% $s_{x^2+y^2}+80\%$ $d_{x^2-y^2}$ (dashed dotted curve), the nesting ridges (dotted) and the gap node peaks with a cross and open circle for pure d wave and 20% $s_{x^2+y^2}$ $+80\%$ $d_{x^2-y^2}$, respectively. The nesting peaks correspond to the intersection of two nesting ridges. Frame (a) is the normal state with $U_c=2.52t$. Frame (b) is the superconducting state for pure d wave with $U_c=2.71t$ and frame (d) is the same but now the gap has 20% $s_{x^2+y^2}$ plus 80% $d_{x^2-y^2}$.

sults for the superconducting state at zero temperature ($T=0$) in the pure d-wave case. The figure is symmetric in q_x and q_y, and the gap node to gap node peak is as large as are the two nesting peaks. The critical value of Coulomb potential is $U_c=2.71t$. Finally, frame 4(d) shows results for a gap with 20% $s_{x^2+y^2}$ and 80% $d_{x^2-y^2}$; U_c has shifted slightly to $2.64t$. The nesting peaks are now quite asymmetric as is the gap node to gap node ridge. We emphasize again that this anisotropy comes completely from gap anisotropy and does not reflect any direct effect of band structure anisotropy. Reducing the damping parameter, Γ, greatly increases the relative height of the gap scattering peak with respect to the nesting peaks. To see a smooth surface, it is necessary to use a much denser mesh.

We turn now to the effect of direct band structure anisotropy on the anisotropy in the susceptibility, i.e., the effect of orthorhombicity on the band structure as opposed to gap anisotropy and to the question of differentiating clearly between these two sources of anisotropy. Figure 5 consists of three frames. The anisotropy parameter δ is 0.25 and $B=0.0$ in the dispersion relation (6). Frame 5(a) shows the corresponding Fermi surface (for a filling of $\langle n\rangle=0.4$) which is elongated along the horizontal axis. The nesting ridges, shown as the dotted curves, also reflect the elongation of the Fermi surface and the tetragonal symmetry seen in frame (a) of Fig. 2 is lost. Frame 5(b) gives the imaginary part of the susceptibility in the superconducting state at $T=0$ for $2\Delta_0=0.4t$, $\omega=0.05t$, $\Gamma=0.05t$, $U=0.0$, with $U_c=2.85t$. The gap node to gap node ridges are just visible in this figure and the nesting peaks are not symmetric in height or position. The one along q_y (right) is higher than the one along q_x (left). Including a finite value of $U=2.7t$ reduces the gap node ridges and emphasizes the anisotropy of the nesting peaks as seen in frame 5(c). The anisotropy of all these figures is due to band structure effect; the gap has pure d-wave symmetry in the superconducting state [frames 5(b) and 5(c)].

In Fig. 6, we show results for the same case as in Fig. 5, i.e., $B=0$ and $\delta=0.25$ in the electronic dispersion (6). We show five pairs of curves. In each set, the upper curve is for momentum along the q_y axis with $q_x=\pi$ and the lower line is

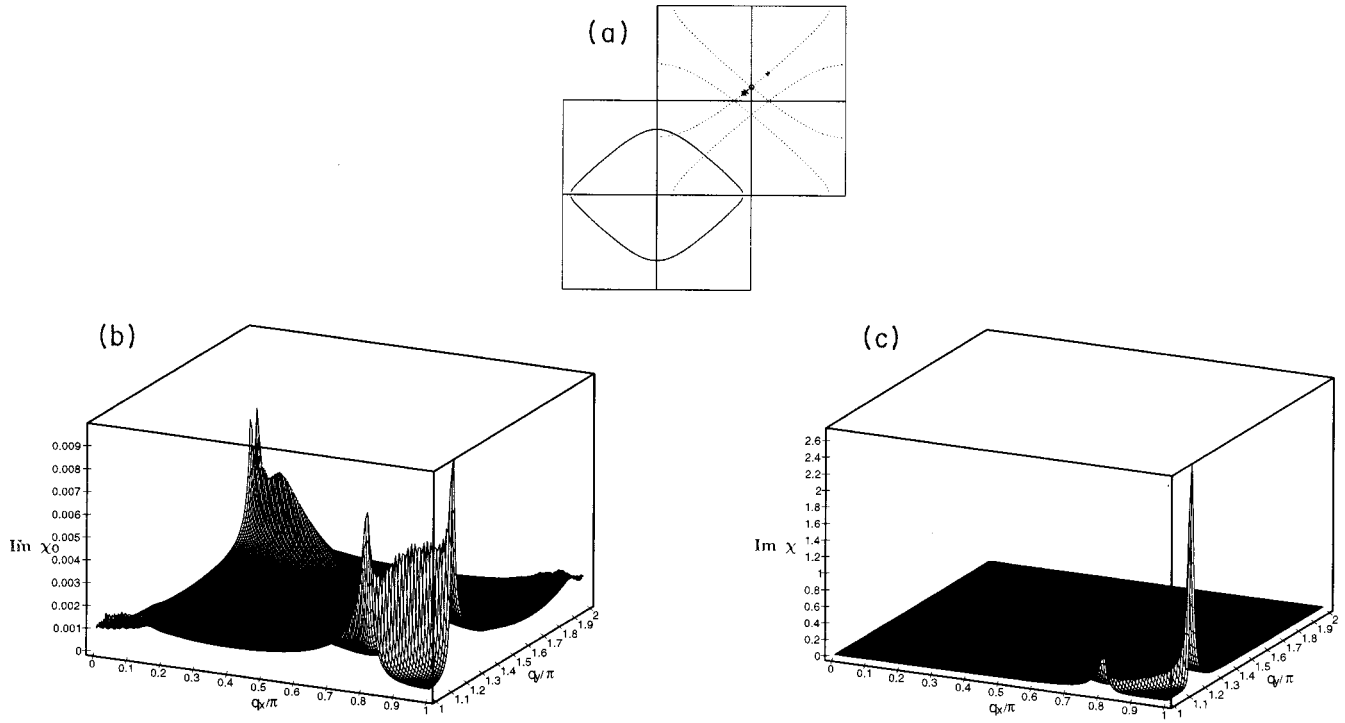

FIG. 5. The parameters are critical temperature $T_c=0.1t$, maximum gap $2\Delta_0=4T_c$, filling $\langle n\rangle=0.4$, second nearest-neighbor hopping $B=0.0$, neutron energy transfer $\omega=0.05t$, and smearing parameter $\Gamma=0.05t$. The number of points used in the Brillouin zone is $(288)^2$ and $\delta=0.25$ in the electronic dispersion Eq. (6) (orthorhombic case) and Coulomb parameter $U_c=2.85t$. Frame (a) shows the Fermi surface (solid curve), the nesting ridges (dotted curve), and the gap node peak for pure d wave (*), 20% extended s-wave admixture ($\times$), 50% ($\bigcirc$) and 80% extended s-wave (+) admixture. Frame (b) is for pure d wave in the superconducting case with Coulomb parameter $U=0.0$. Frame (c) is also for pure d-wave but now $U=2.70t$.

along q_x with $q_y=\pi$. Each set of curves is displaced upward along the vertical axis for viewing convenience. The lowest set of curves is for the normal state at temperature $T=0.1t$ and now shows a different profile between x and y direction because of band structure anisotropy. This is to be contrasted with the tetragonal case shown in Fig. 3 where no such anisotropy is seen. The next four pairs of curves are all for the superconducting state at zero temperature with $s_{x^2+y^2}=0$, 20%, 50%, and 80%, respectively. The anisotropy between the peaks in q_x and q_y direction is further increased as the amount of extended s-wave admixture in the gap function is increased. This anisotropy is added to the anisotropy seen in the normal state which has its origin solely in the band anisotropy of $\epsilon_{\mathbf{k}}$ in Eq. (6). This is the characteristic that should be looked for in identifying $s_{x^2+y^2}$ admixtures to a pure $d_{x^2-y^2}$ gap in an orthorhombic system.

Figure 7 deals with a similar case to that of Fig. 5 but now the second nearest-neighbor hopping is finite, namely $B=0.45$ (often used to model YBCO). In contrast to the results shown in Fig. 4 for the equivalent tetragonal case, we have now included some band structure anisotropy in the dispersion relation (6) and $\delta=0.25$. This distorts the Fermi surface which is now open in the horizontal direction of frame (a) of Fig. 7 while remaining closed in the vertical direction (solid curve) in the first Brillouin zone. The nesting ridges, shown as the dotted curves in an extended Brillouin zone centered about $\mathbf{q}=(\pi,\pi)$, are correspondingly changed as compared with frame (c) of Fig. 4. Also, the maximum of the gap node to gap node Fermi surface scattering peak is shifted to follow the new nesting ridges. The remaining four frames show the imaginary part of the spin susceptibility as a function of momentum (q_x,q_y) for filling $\langle n\rangle=0.4$, temperature $T=0$, $\omega=0.05t$, $\Gamma=0.01t$, and number of sampling points equal to N^2 with $N=330$. The maximum gap was set at $2\Delta_0=0.4t$. Frame 7(b) is for the case of a pure d-wave gap with Coulomb potential $U=0.0t$. Here the critical value of U is $U_c=2.70t$. Frame 7(c) is Coulomb enhanced with $U=2.65t$. It is clear that the band structure anisotropy $\delta=0.25$ has given rise to anisotropy in the nesting peaks which is greatly enhanced when U is finite over its value when $U=0$, i.e., bare susceptibility χ_0 of Eq. (1). Less anisotropy is clearly seen in frames 7(d) and 7(e) which contain a 20% admixture of $s_{x^2+y^2}$ to the gap. In frame 7(d), $U=0t$ and $U_c=2.77t$ while for frame 7(e) $U=2.65t$. Even for the Coulomb enhanced case, the gap node to gap node scattering ridge is seen to remain large and comparable in size to the highest of the two nesting peaks. As compared with the pure d-wave case, there is less difference between the peak heights of the nesting structures—this is due to the gap anisotropy. Note that even in the pure $d_{x^2-y^2}$ case [frames 7(b) and 7(c)] the highest nesting peak (left) is the opposite to that seen in Figs. 2(c), 2(d), 2(e), 4(d), and 5(b) (right). The movement of the gap scattering peak towards the right hand peak serves to reduce the relative anisotropy in the nesting peak heights (i.e., mixing of the $s_{x^2+y^2}$ irreducible representation of the tetragonal crystal point group with the $d_{x^2-y^2}$

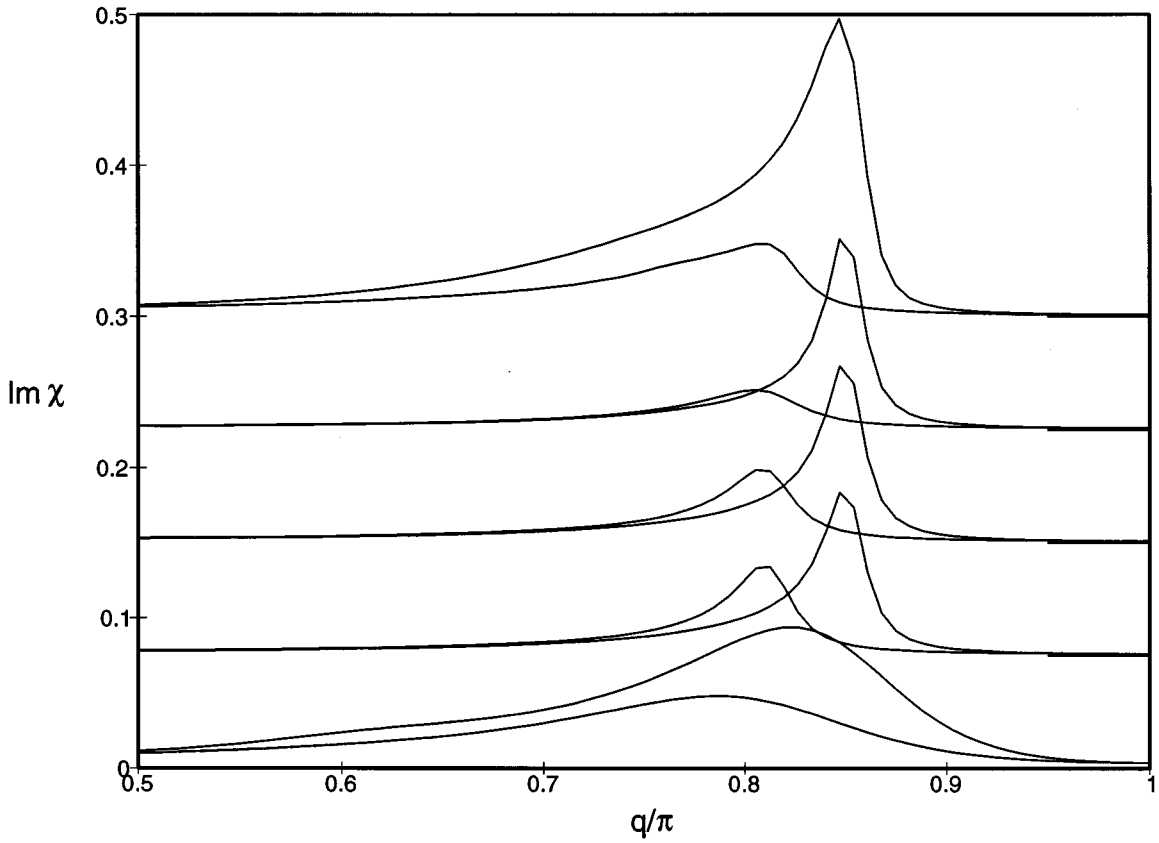

FIG. 6. The parameters are critical temperature $T_c=0.1t$, maximum gap $2\Delta_0=4T_c$, filling $\langle n\rangle=0.4$, second nearest-neighbor hopping $B=0$, but with $\delta=0.25$ in Eq. (6), i.e., an orthorhombic case. The neutron energy transfer $\omega=0.05t$ and the smearing $\Gamma=0.05t$. The number of points used in the Brillouin zone was $(288)^2$. Each set of two curves is displaced upward for clarity by the same amount (0.75). The graph gives the imaginary part of the susceptibility as a function of momentum q/π. The upper line is along q_y with $q_x=\pi$ and the lower curve along q_x with $q_y=\pi$. The lowest set of curves apply to the normal state at $T=T_c$. All others are for the superconducting state at $T=0$. Second from bottom is pure d wave, next is 20% $s_{x^2+y^2}+80\%$ $d_{x^2-y^2}$, next is 50% of each and the top set, 80% $s_{x^2+y^2}+20\%$ $d_{x^2-y^2}$.

representation). Increasing U, for 0% and 20% $s_{x^2+y^2}$ admixture greatly increases the anisotropy in the height of the peaks. For the equal admixture, however, there is a reduction in the relative heights. This is due to the commensurate gap node peak and (right) nesting peak.

IV. DISCUSSION AND CONCLUSIONS

Using a tight-binding single band model, we have calculated the spin susceptibility enhanced by constant Hubbard U for normal and superconducting states of a d-wave superconductor. Particular attention was paid to the nesting peaks and gap node to gap node scattering peaks in the superconducting state, with and without Stoner enhancement. First, we studied the case of a tetragonal lattice with the aim of understanding how an admixture of a component of $s_{x^2+y^2}$ symmetry to a gap of $d_{x^2-y^2}$ symmetry changes the principle features of the imaginary part of the susceptibility in momentum space. It was found that as the $s_{x^2+y^2}$ component is introduced, the four incommensurate nesting peaks, which are all identical in the pure d-wave case, form pairs. The height of one pair is lowered while that of the other pair increases in a specific way. Observation of this height difference, which exists only for the superconducting state, should, in principle, allow the amount of $s_{x^2+y^2}$ admixture to the d-wave gap to be measured. Such anisotropy in the nesting peaks, which is not present in the normal state, may have been measured in the experiments of Mason *et al.*[20] The gap node to gap node scattering ridges also get distorted by admixing an $s_{x^2+y^2}$ component to a d-wave gap and the tetragonal symmetry is lost. The effects described above, which are present for $U=0$, i.e., no Coulomb enhancement of the susceptibility, are even more pronounced when the Stoner enhancement is taken into account. The relative difference in height of the two pairs of nesting peaks gets further enhanced. This effect is largest at 50% $s_{x^2+y^2}$ admixture, except when $B\neq 0\neq\delta$—then increasing U reduces the relative height difference. This effect is in addition to the general increase in the spin susceptibility that is expected as the antiferromagnetic boundary is approached from the metallic side.

As a first approximation, a simple one band model is also used to describe an orthorhombic lattice. In our simplified model, the x and y directions are made different by assuming that the nearest-neighbor hopping parameter are different in

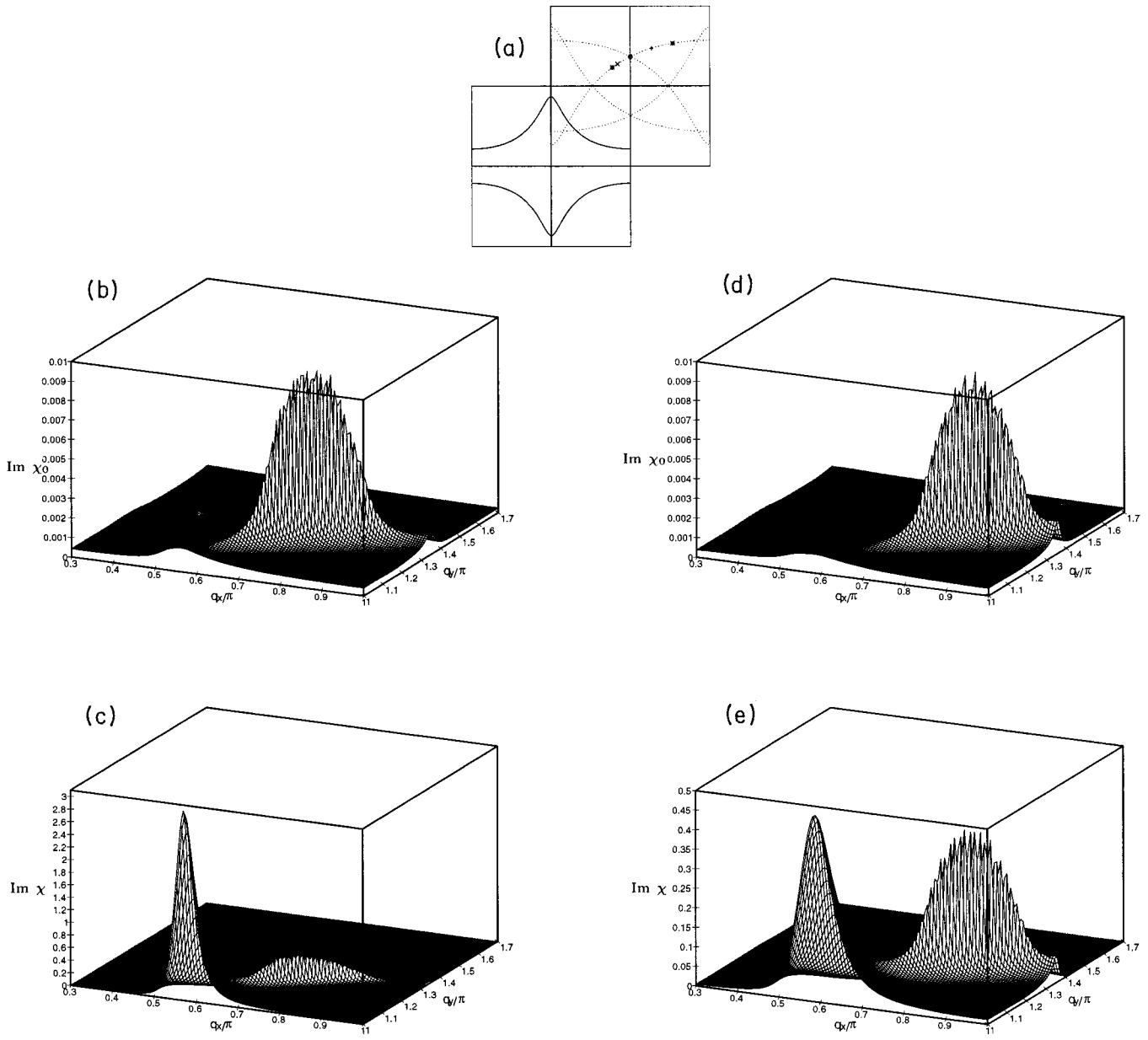

FIG. 7. The parameters are critical temperature $T_c=0.1t$, maximum gap $2\Delta_0=4T_c$, filling $\langle n\rangle=0.4$ second nearest-neighbor hopping $B=0$ on an orthorhombic lattice (δ=.25), neutron energy transfer $\omega=0.05t$, and smearing parameter $\Gamma=0.01t$. The number of point samples in the Brillouin zone is $(330)^2$. Frame (a) gives the Fermi surface (solid curve) and the nesting ridges (dotted curves). The nesting peaks are centered around the crossing point of two nesting ridges. The points indicated trace the gap node peak position; *, pure d wave; ×, 20% $s_{x^2+y^2}+80\%$ $d_{x^2-y^2}$;○, 50% $s_{x^2+y^2}+50\%$ $d_{x^2-y^2}$; and +, 80% $s_{x^2+y^2}+20\%$ $d_{x^2-y^2}$ and second * pure $s_{x^2+y^2}$. The four frames (b) to (e) give plots of the imaginary part of the spin susceptibility as a function of momentum in the first Brillouin zone. Frame (b) is for Coulomb potential $U=0$ while in frame (c) its value is set at $U=2.65t$ and both frames apply for pure d wave with $U_{\rm crit}=2.70t$. The other two frames, (d) and (e), are similar but the gap is 20% $s_{x^2+y^2}+80\%$ $d_{x^2-y^2}$ with $U=0$ in (d) and $U=2.65t$ in (e); $U_{\rm crit}=2.77t$.

each of these two directions. This band structure anisotropy distorts the Fermi surface itself which then ceases to have tetragonal symmetry. This leads to a difference in the height of the nesting peak in the k_x and k_y direction. It is important to note, however, that this band anisotropy as opposed to gap anisotropy persists in the normal state, and that in the superconducting state, the band structure anisotropy is further enhanced by including an extended s-wave component to the otherwise d-wave gap. It should therefore be possible to differentiate between these two sources of anisotropy in the

momentum space structure of the spin susceptibility. Such experiments can, in principle, help determine the symmetry of the gap.

Inclusion of next-nearest-neighbor hopping on an orthorhombic lattice reverses the anisotropy in height of the two pairs of nesting peaks. Increasing the admixture of extended *s*-wave gap with *d*-wave gap tends to reduce this relative anisotropy. Thus, if the nesting peaks are less anisotropic in the superconducting state than in the normal state, there is next nearest-neighbor hopping on an orthorhombic lattice.

ACKNOWLEDGMENTS

Research supported in part by the Natural Sciences and Engineering Research Council of Canada (NSERC) and by the Canadian Institute for Advanced Research (CIAR). We thank T. E. Mason for an illuminating discussion.

[1] A. J. Millis, H.Monien, and D. Pines, Phys. Rev. B **42**, 167 (1990).
[2] P. Monthoux and D. Pines, Phys. Rev. Lett. **69**, 961 (1992).
[3] P. Monthoux and D. Pines, Phys. Rev. B **47**, 6069 (1993).
[4] D. Pines, J. Phys. Chem. Solids **54**, 1447 (1993).
[5] D. J. Scalapino, J. Phys. Chem. Solids **54**, 1433 (1993).
[6] P. W. Anderson, J. Phys. Chem. Solids **54**, 1457 (1993).
[7] St. Lenck, J. P. Carbotte, and R. C. Dynes, Phys. Rev. B **50**, 10 149 (1995); **49**, 9111 (1995).
[8] G. Aeppli *et al.*, Phys. Rev. Lett. **62**, 2052 (1989).
[9] P. C. Hammel *et al.*, Phys. Rev. Lett. **63**, 1992 (1989).
[10] S. W. Cheong *et al.*, Phys. Rev. Lett. **67**, 1791 (1991).
[11] J. Rossat-Mignod *et al.*, Physica (Amsterdam) B **169**, 58 (1991).
[12] J. Rossat-Mignod *et al.*, Physica C **185–189**, 86 (1991).
[13] G. Shirane *et al.*, Phys. Rev. Lett. **63**, 330 (1989).
[14] T. R. Thurston *et al.*, Phys. Rev. B **40**, 4585 (1989).
[15] R. J. Birgeneau *et al.*, Z. Phys. B Condens. Matter **87**, 15 (1992).
[16] J. M. Tranquada *et al.*, Phys. Rev. B **46**, 5561 (1992).
[17] T. E. Mason, G. Aeppli, and H. A. Mook, Phys. Rev. Lett. **68**, 1414 (1992).
[18] T. R. Thurston *et al.*, Phys. Rev. B **46**, 9128 (1992).
[19] B. J. Sternlieb *et al.*, Phys. Rev. B **47**, 5320 (1993).
[20] T. E. Mason, G. Aeppli, S. M. Hayden, A. P. Ramirez, and H. A. Mook, Phys. Rev. Lett. **71**, 919 (1993).
[21] H. F. Fong *et al.*, Phys. Rev. Lett. **75**, 316 (1995).
[22] G. Shirane *et al.*, Physica B **197**, 158 (1994).
[23] P. Dai, H. A. Mook, G. Aeppli, F. Dogan, K. Salama, and D. Lee (unpublished).
[24] H. J. Schulz, Phys. Rev. Lett. **64**, 1445 (1990).
[25] N. Bulut, H. Hone, D. J. Scalapino, and N. E. Bickers, Phys. Rev. Lett. **64**, 2723 (1990).
[26] L. Chen, C. Bourbonnais, T. Li, and A. M. Tremblay, Phys. Rev. Lett. **66**, 369 (1991).
[27] J. Ruvalds, C. T. Rieck, J. Zhang, and A. Virosztek, Science **256**, 1664 (1992).
[28] P. Benard *et al.*, Phys. Rev. B **47**, 589 (1993).
[29] P. B. Littlewood, J. Zaanen, G. Aeppli, and H. Monien, Phys. Rev. B **48**, 487 (1993).
[30] N. Bulut and D. J. Scalapino, Phys. Rev. B **47**, 3419 (1993); **50**, 16 078 (1994).
[31] S. M. Quinlan and D. J. Scalapino, Phys. Rev. B **51**, 497 (1995).
[32] F. Marsiglio, Phys. Rev. B **47**, 11 555 (1993).
[33] M. Lavagna and G. Stemmann, Phys. Rev. B **49**, 4235 (1994).
[34] Y. Zha, K. Levin, and Qimiao Si, Phys. Rev. B **47**, 9124 (1993).
[35] G. Stemmann, C. Pépin, and M. Lavagna, Phys. Rev. B **50**, 4075 (1994).
[36] Qimiao Si *et al.*, Phys. Rev. B **47**, 9055 (1993).
[37] J. P. Lu, Phys. Rev. Lett. **68**, 125 (1992); Mod. Phys. Lett. B **6**, 547 (1992).
[38] N. Bulut and D. J. Scalapino, Phys. Rev. B **45**, 2371 (1992).
[39] H. Monien and D. Pines, Phys. Rev. B **41**, 6297 (1990).
[40] N. Bulut and D. J. Scalapino, Phys. Lett **68**, 706 (1992).
[41] J. P. Lu, Mod. Phys. Lett. B **6**, 547 (1992).
[42] D. Thelen, D. Pines, and J. P. Lu, Phys. Rev. B **47**, 9151 (1993).
[43] P. Benard, Liang Chen, and A. M. Tremblay, Phys. Rev. B **47**, 15 217 (1993).
[44] Q. P. Li, B. E. C. Koltenbah, and R. Joynt, Phys. Rev. B **48**, 437 (1993).
[45] J. F. Annett and N. Goldenfeld, J. Low Temp. Phys. **81**, 197 (1992).
[46] B. G. Levi, Phys. Today **46** (5), 17 (1993).
[47] W. N. Hardy, D. A. Bonn, D. C. Morgan, R. Liang, and K. Zhang, Phys. Rev. Lett. **70**, 3999 (1993).
[48] D. A. Bonn *et al.*, Phys. Rev. B **47**, 11 314 (1993).
[49] D. A. Bonn, P. Dosanjh, R. Liang, and W. N. Hardy, Phys. Rev. Lett. **68**, 2390 (1992).
[50] K. Zhang, D. A. Bonn, R. Liang, D. J. Barr, and W. N. Hardy, Appl. Phys. Lett. **62**, 3019 (1993).
[51] D. A. Bonn, K. Zhang, R. Liang, D. J. Barr, and W. N. Hardy, J. Supercond. **6**, 219 (1993).
[52] W. N. Hardy, S. Kamal, D. A. Bonn, K. Zhang, R. Liang, E. Klein, D. C. Morgan, and D. J. Barn, Physica B **197**, 609 (1994).
[53] H. Ding, J. C. Campuzano, K. Gofron, C. Gu, R. Liu, B. W. Veal, and G. Jennings, Phys. Rev. B **50**, 1333 (1994).
[54] G. C. Olson *et al.*, Science **245**, 731 (1989).
[55] Z. X. Shen *et al.*, Phys. Rev. Lett. **70**, 1553 (1993).
[56] D. S. Dessau, Z. X. Shen, B. O. Wells, and W. E. Spicer, J. Phys. Chem. Solids **52**, 1401 (1991).
[57] Jian Ma, C. Quitmann, R. J. Kelley, H. Berger, G. Margaritondo, and M. Onellion, Science **267**, 862 (1995).
[58] Y. Hwu *et al.*, Phys. Rev. Lett. **67**, 2573 (1991).
[59] R. J. Kelley, J. Ma, G. Margaritondo, and M. Onellion, Phys. Rev. Lett. **71**, 4051 (1993).
[60] D. S. Desseau *et al.*, Phys. Rev. Lett. **66**, 2160 (1991).
[61] H. Ding and J. C. Campuzano *et al.*, Phys. Rev. Lett. **50**, 1333 (1994).
[62] H. Ding, J. C. Campuzano, A. F. Bellman, T. Yokoya, M. R. Norman, M. Randeria, T. Takahashi, H. Katayama-Yoshida, T. Mochiku, K. Kadowaki, and G. Jennings, Phys. Rev. Lett. **74**, 2784 (1995).
[63] D. A. Wollman, D. J. Van Harlingen, W. C. Lee, D. M. Ginsberg, and A. J. Leggett, Phys. Rev. Lett. **71**, 2134 (1993).
[64] P. Chaudhari and Shawn Yu Lin, Phys. Rev. Lett. **72**, 1084 (1994).
[65] A. G. Sun, D. A. Gajewki, M. B. Maple, and R. C. Dynes, Phys. Rev. Lett. **72**, 2267 (1994).
[66] S. Chakravarty, A. Sudbo, P. W. Anderson, and S. Strong, Science **261**, 337 (1993).
[67] P. B. Littlewood and C. M. Varma, Phys. Rev. B **46**, 405 (1992).
[68] A. A. Abrikosov, Physica C **182**, 191 (1991).

[69] T. A. Friedmann *et al.*, Phys. Rev. B **42**, 6217 (1990).
[70] R. C. Yu, M. B. Salamon, Jian Ping Lu, and W. C. Lee, Phys. Rev. Lett. **69**, 1431 (1992).
[71] K. Zhang, D. A. Bonn, S. Kamal, R. Liang, D. J. Baar, W. N. Hardy, D. Basov, and T. Timusk, Phys. Rev. Lett. **73**, 2484 (1994).
[72] C. O'Donovan, D. Branch, J. P. Carbotte, and J. Preston, Phys. Rev. B **51**, 6588 (1995).
[73] C. O'Donovan and J. P. Carbotte, Phys. Rev. B **52**, 4568 (1995).
[74] D. Branch and J. P. Carbotte, Phys. Rev. B **52**, 603 (1995).
[75] H. Krakauer, W. E. Pickett, and R. E. Cohen, Supercond. **1**, 111 (1988).
[76] W. E. Pickett, R. E. Cohen, and H. Krakauer, Phys. Rev. B **42**, 8764 (1990).
[77] W. E. Pickett, H. Krakauer, R. E. Cohen, and D. J. Singh, Science **255**, 1 (1992).
[78] H. Haghighi *et al.*, Phys. Rev. Lett. **67**, 382 (1991).
[79] A.J. Arko *et al.*, Phys. Rev. B **40**, 2268 (1989).
[80] J. C. Campuzano *et al.*, Phys. Rev. Lett. **64**, 2308 (1990).
[81] N. Schroeder *et al.*, Phys. Rev. **47**, 5287 (1993).